A Brain-Computer Interface Based on a Few-Channel EEG-fNIRS Bimodal System

SHENG GE[1], QING YANG[1], RUIMIN WANG[2], PAN LIN[1], JUNFENG GAO[3], YUE LENG[1], YUANKUI YANG[1], AND HAIXIAN WANG[1], (Senior Member, IEEE)

[1]Key Laboratory of Child Development and Learning Science, Ministry of Education, Research Center for Learning Science, Southeast University, Nanjing 210096, China
[2]Graduate School of Systems Life Sciences, Kyushu University, Fukuoka 8190395, Japan
[3]Key Laboratory of Cognitive Science of State Ethnic Affairs Commission, College of Biomedical Engineering, South-Central University for Nationalities, Wuhan 430074, China

Corresponding author: H. Wang (hxwang@seu.edu.cn)

ABSTRACT With the development of the wearable brain–computer interface (BCI), a few-channel BCI system is necessary for its application to daily life. In this paper, we proposed a bimodal BCI system that uses only a few channels of electroencephalograph (EEG) and functional near-infrared spectroscopy (fNIRS) signals to obtain relatively high accuracy. We developed new approaches for signal acquisition and signal processing to improve the performance of this few-channel BCI system. At the signal acquisition stage, source analysis was applied for both EEG and fNIRS signals to select the optimal channels for bimodal signal collection. At the feature extraction stage, phase-space reconstruction was applied to the selected three-channel EEG signals to expand them into multichannel signals, thus allowing the use of the traditional effective common spatial pattern to extract EEG features. For the fNIRS signal, the Hurst exponents for the selected ten channels were calculated and composed of the fNIRS data feature. At the classification stage, EEG and fNIRS features were joined and classified with the support vector machine. The averaged classification accuracy of 12 participants was 81.2% for the bimodal EEG-fNIRS signals, which was significantly higher than that for either single modality.

INDEX TERMS BCI, EEG, fNIRS, phase-space reconstruction, common spatial pattern, data fusion, support vector machine.

I. INTRODUCTION

Brain-computer interfaces (BCIs) were developed to allow communication between human thought processes and a computer, with the aim of assisting disabled patients with motor function impaired as a result of disease or injury, but whose mental functions are not severely affected [1]–[3]. The major noninvasive modalities for BCI include electroencephalography (EEG) [4]–[7], magnetoencephalography (MEG) [8], [9], functional magnetic resonance imaging (fMRI) [10], [11], and functional near-infrared spectroscopy (fNIRS) [12]–[14]. Each modality has specific advantages and limitations. The optimal selection for a BCI system reflects the cost of the equipment, as well as the spatial and temporal resolution required for the specific application.

In principle, MEG and fMRI provide the optimal basis for a BCI. However, these techniques are expensive, non-portable, and require the user to remain stationary during measurement, making MEG and fMRI unsuitable for BCI applications. EEG is noninvasive, economical, portable, and has a high temporal resolution. However, EEG also has some disadvantages, including low spatial resolution, low signal strength, and susceptibility to electrical noise. fNIRS is a noninvasive method for measuring the concentration changes of oxygenated hemoglobin (HbO) and deoxygenated hemoglobin (HbR) with near-infrared-range light (650–1000 nm) [12], [15], [16]. fNIRS uses multiple emitter-detector pairs operating with near-infrared (NI) light at two or more different wavelengths. Because the skin, scalp and skull are relatively transparent to NI light, the light transmits into the brain tis-

sues. The NI light is emitted at the skin of the head, transmits through the skull into the brain; then diffuses through the brain tissues due to photon scattering. However, a portion of NI light exits the scalp after passing through the cortical brain region, where the HbO and HbR chromophores in the light-path absorb light with different absorption coefficients. The exited photons are detected using strategically positioned detectors, and the intensity of the detected light is used to calculate HbO and HbR concentration changes (ΔHbO and ΔHbR) along the photon path by the Beer-Lambert law [12], [17]. Following neural activation, fNIRS measures the ΔHbO and ΔHbR in the outer layers of the cortex. The concentration of HbO is expected to increase after focal activation of the cortex due to higher blood flow, whereas HbR is washed out and decreases [18]. Thereby, fNIRS measures a comparable effect to the blood oxygenation level dependent (BOLD) contrast in fMRI. fNIRS has relatively low cost, portability, safety, low noise (compared to fMRI), and is easy to use. More importantly, fNIRS has high spatial resolution and is more resistant to electrical noise. For these reasons, fNIRS-based BCIs have recently become widely used [12]–[14], [19]–[21].

Motor imagery is one of the classic and widely used BCI paradigms in BCI research. It is a mental process by which an individual rehearses or simulates a given action in their mind [6], [22]. Beisteiner *et al.* [23] demonstrated that brain activation during a motor imagery was similar to that observed during the associated motor execution (overt body movement). Further, motor imagery was shown to work well in previous EEG-based BCI studies [6], [24]–[28]. More recently, motor imagery has also been used in fNIRS-based BCI systems [14], [19], [21], [29]–[32]. For example, Sitaram *et al.* [14] reported an 89.1% accuracy for classifying fNIRS signals arising from right- and left-hand motor imagery, whereas Naseer et al. reported average classification accuracies of 77.56% and 87.28% for right- and left-wrist motor imageries, respectively [21]. Further, Takahashi *et al.* [32] showed good discrimination results for task categories from the motor area, prefrontal area, and frontal lobe data using multichannel fNIRS.

The majority of EEG- and fNIRS-based BCIs are based on multichannel data. However, the higher the number of channels, the reduced portability and comfort of the BCI, and the longer the preparation time. Thus, BCI systems that achieve relatively high classification accuracy using only a few signal channels are required. Every neuroimaging method has specific limitations (e.g., spatial resolution for EEG; temporal resolution for fNIRS). However, the use of multi-modal data acquisition can partly overcome these limitations by focusing on the strengths of the individual modalities. More importantly, the information acquired from multiple sources can be used to increase data quality and quantity. Although a few studies have reported bimodal BCI devices, most of them are multichannel [33]–[40]. Thus, in the present study, with the aim of developing a portable and wearable BCI device for the wider population, we used bimodal EEG-fNIRS data acquisition to develop a few-channel BCI system.

## II. MATERIALS AND METHODS

A. PARTICIPANTS

Twelve healthy participants voluntarily participated in the present study (six males, six females, mean age 23 years). No participants had any known history of neurological disorders. All participants had normal or corrected-to-normal visual acuity, had no previous experience with BCI operation nor EEG/fNIRS recordings, and were right-handed as confirmed by the Edinburgh Handedness Inventory. All participants gave written informed consent for the experimental procedures, which were approved by the Ethics Committee of Affiliated Zhongda Hospital, Southeast University (2016ZDSYLL002.0).

FIGURE 1. EEG-fNIRS bimodal experimental environment.

B. EXPERIMENTAL PROCEDURE

The experiment was performed in a quiet room to reduce disturbance from the environment. The participant sat in a comfortable chair with her/his head on a chin rest (Fig.1). A computer display on which stimuli were displayed was set 80 cm away from the participant. The participant was asked to relax for at least 5 min prior to the experiment, and to remain relaxed throughout the experiment. A schematic of the protocol is shown in Fig.2. Each experiment consisted of three sessions, and each session comprised 20 trials, with a 2 min rest period between sessions (total of 60 trials in one experiment). Refer to Fazli's study [39], a 10 s long motor imagery task was used in the present study to get sufficient data for classification. Each trial started with a pre-rest block during which the participant stayed still for 5 s. This was followed by the appearance of a cross on the screen for 2 s, indicating to the participant to prepare for the motor imagery task. Next, the participant performed the motor imagery task for 10 s, as indicated by an arrow on the computer screen. A left-pointing arrow indicated a left-hand motor imagery task, and vice versa. Participants were asked to perform the same type of hand movement during the motor imagery task. After the motor imagery task block, the participant underwent
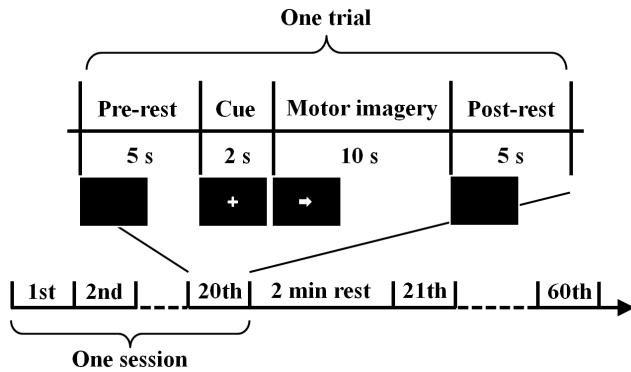
FIGURE 2. Experimental paradigm for EEG-fNIRS signal collection. Each experiment consisted of three sessions, and each session comprised 20 trials. Each trial consisted of a pre-rest block of 5 s, a preparation block of 2 s, a motor task block of 10 s, and a post-rest block of 5 s. During the task, participants imagined hand movement of the specified hand over the 10 s duration of the task block.

a post-rest period for 5 s. Thus, one experiment lasted for 26 min.

C. DATA ACQUISITION

EEG and fNIRS data were recorded simultaneously to compose an EEG-fNIRS bimodal BCI system in the present study. EEG data were collected using a 64-channel Neuroscan system (Neuroscan Synamps amplifier; Scan 4.5 Compumedics Corp., El Paso, TX, USA) according to the international 10–20 system (Fig.3a), with the reference on the left mastoid. Eye blinks were monitored with electrodes located above and below the right eye. The horizontal electrooculogram (EOG) was recorded from electrodes placed 1.5 cm lateral to the left and right external canthi. All electrode impedances were maintained below 5 $k\Omega$. EEG and EOG data were amplified using a 0.05–70 Hz bandpass filter, and a notch filter allowed suppression of line noise. Data were continuously sampled at 1000 Hz.

fNIRS recording was performed via 52-channel LABNIRS (Shimadzu Co., Ltd., Kyoto, Japan). This system used three wavelengths (780, 805, and 830 nm) of continuous near-infrared light. The HbO, HbR and total hemoglobin (total-Hb = HbO + HbR) concentration changes during the motor imagery tasks were recorded. fNIRS optodes have been placed over the bilateral primary motor cortex (Fig.3b), which is known to be the area activated by motor imagery [41], [42]. A pair of emitter and detector optodes formed one fNIRS channel, and an emitter-detector separation of around 3 cm was used [43]. Eleven emitter and 11 detector optodes resulting in a total of 31 channels were placed around the C3-Cz-C4 areas. fNIRS data were acquired at a sampling rate of 28 Hz.

D. SOURCE ANALYSIS AND CHANNEL SELECTION

To improve the performance of our proposed few-channel EEG-fNIRS BCI system, we optimized the configuration of the EEG and fNIRS channels (i.e., selected the best channels to build a few-channel system for data collection). To achieve this, we performed source analysis of the brain

activations for motor imagery tasks for both 64-channel EEG and 31-channel fNIRS, respectively (Fig.4). Before performing source analysis, data pre-processing was applied for both EEG and fNIRS data. For EEG data, a bandpass filter was used to filter the EEG data between 6 and 30 Hz. Independent component analysis (ICA) was performed with the ICALAB toolbox [44] to find an unmixing matrix that linearly decomposed the 64-channel EEG data into 64 independent components (ICs). ICs that exhibited a high correlation with EOG signals were considered responsible for EOG artifacts, and were set to zero vectors, whereas all other ICs were projected back onto the scalp to provide an EEG free of EOG artifacts [45], [46]. To remove noise and artifacts, all data were smoothed with a window of 101 data points. The data from 2 s to 8 s during the motor imagery period were selected for analysis. For fNIRS, the data were bandpass filtered between 0.02 and 0.1 Hz. The baseline period was defined from -2 s to 0 s before motor imagery task stimulus, and the mean value of the baseline was calculated for every trial. fNIRS data for all trials were corrected by subtracting the mean value of baseline.

For EEG source analysis, we first used Matlab (2013a) (The MathWorks, Natick, MA, USA) to calculate the grand average for 12 participants. Next, a standardized low-resolution electrical tomographic analysis (sLORETA) software [47] was used on the 12-participant grand average, which addressed the inverse problem by calculating the current source density (CSD) from electrical signals recorded from the scalp to estimate the source location. The solutions were based on the Talairach cortical probability brain atlas, digitized at the Montreal Neurological Institute (MNI). The electrode locations were co-registered between both the spherical model (BESA) and the realistic head geometry [48]. The inverse weight projections from the original EEG channels for each component contributing to the temporal *a*-clusters were exported into sLORETA. Cross-spectra were computed and mapped to the Talairach atlas and cross-registered with the MNI coordinates, resulting in CSD estimates for each contributing component. The statistical significance of the CSD was analyzed with the sLORETA software package.

For fNIRS source analysis, previous studies have reported that HbO concentration exhibits a greater, more significant change during mental tasks than HbR concentration [19], [20]. Thus, we used the 12-participant grand average (calculated with Matlab) of the HbO signal for source analysis. Five anatomical landmarks (nasion, inion, Cz, and left and right preauricular points) and fNIRS optodes (11 emitters, 11 detectors) were digitized using a 3D digitizer (FASTRAK; Polhemus, Colchester, VT, USA). Coordinates of the channels in real space were automatically calculated as intermediate points between the emitters and detectors. The location of each fNIRS channel and the topographical maps of the changes in HbO concentration were then superimposed onto the surface of the MNI standard 3D head model via FUSION 3D imaging software (Shimadzu Co., Ltd.).
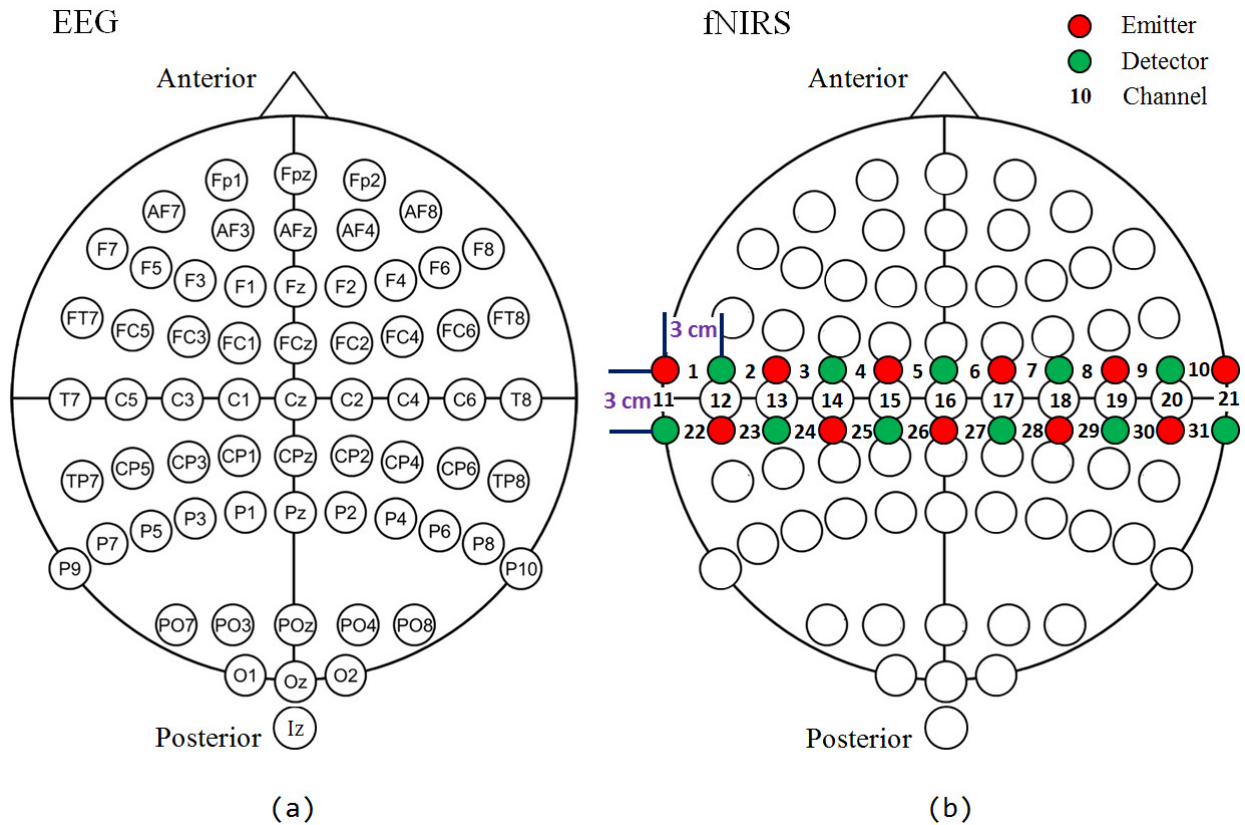
FIGURE 3. Arrangement of EEG and fNIRS channels. (a) 64 EEG channel arrangement based on the international 10–20 system. (b) Probe arrangement for fNIRS. The optodes were arranged above the premotor cortex and the motor cortex. A pair of emitter and detector optodes formed one fNIRS channel. Eleven emitters and 11 detectors in the arrangement resulted in a total of 31 channels.
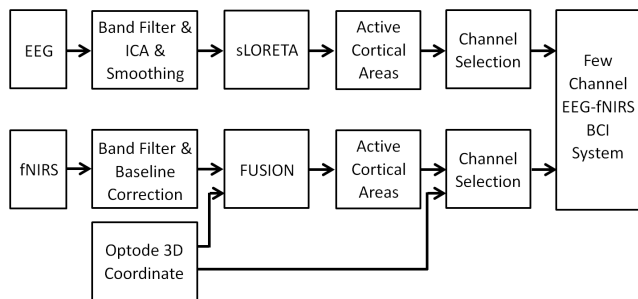
FIGURE 4. The procedure for channel selection.

Based on source analysis results for EEG (Fig.5) and fNIRS (Fig.6), the supplementary motor area and the motor area were the most activated. Therefore, channels from this location were chosen for the few-channel EEG-fNIRS BCI system. C3, Cz, and C4 in the 10–20 system were selected as the EEG channels (Fig.3a), whereas six pairs of emitter and detector optodes around C3 and C4 (see Fig.3b; channels 3, 4, 14, 24 and 25 around C3; channel 7, 8, 18, 28 and 29 around C4, respectively) were selected as the fNIRS channels. This channel selection is consistent with previous studies [49].

E. EEG FEATURE EXTRACTION
The general procedure for bimodal BCI is shown in Fig.7. EEG data were obtained from the selected C3, Cz, and,

C4 channels. As our aim was to distinguish motor imagery using only a few channels, it was important to extract more information from these channels. Thus, we used phase-space reconstruction (PSR) to obtain more detailed characteristics [50]. By performing PSR, a few-channel time-varying signal can be converted into multiple time-varying signals. This channel-increasing method allows previous multichannel BCI approaches, such as the common spatial pattern (CSP), a powerful technique that is normally unsuitable for few-channel signals [51], to be applied to the few-channel method.

Time delay is the most popular method used to reconstruct the phase space [52], [53]. This technique is based on the concept that a scalar (or single-variable) time series x_s, where $s = 1, 2, \ldots, N$ (N is the sample size), can be reconstructed in a multi-dimensional phase space to represent the underlying dynamics, according to:

$$X = [X_1 \quad X_2 \quad \ldots \quad X_M]$$
$$= \begin{bmatrix} x_1 & x_2 & \ldots & x_M \\ x_{1+\tau} & x_{2+\tau} & \ldots & x_{M+\tau} \\ \vdots & \vdots & \ldots & \vdots \\ x_{1+(m-1)\tau} & x_{2+(m-1)\tau} & \ldots & x_N \end{bmatrix} \quad (1)$$

where $M = N - (m-1)\tau$, m is the embedding dimension of the vector X_k, $k = 1, 2, \ldots, M$, and τ is the embedding
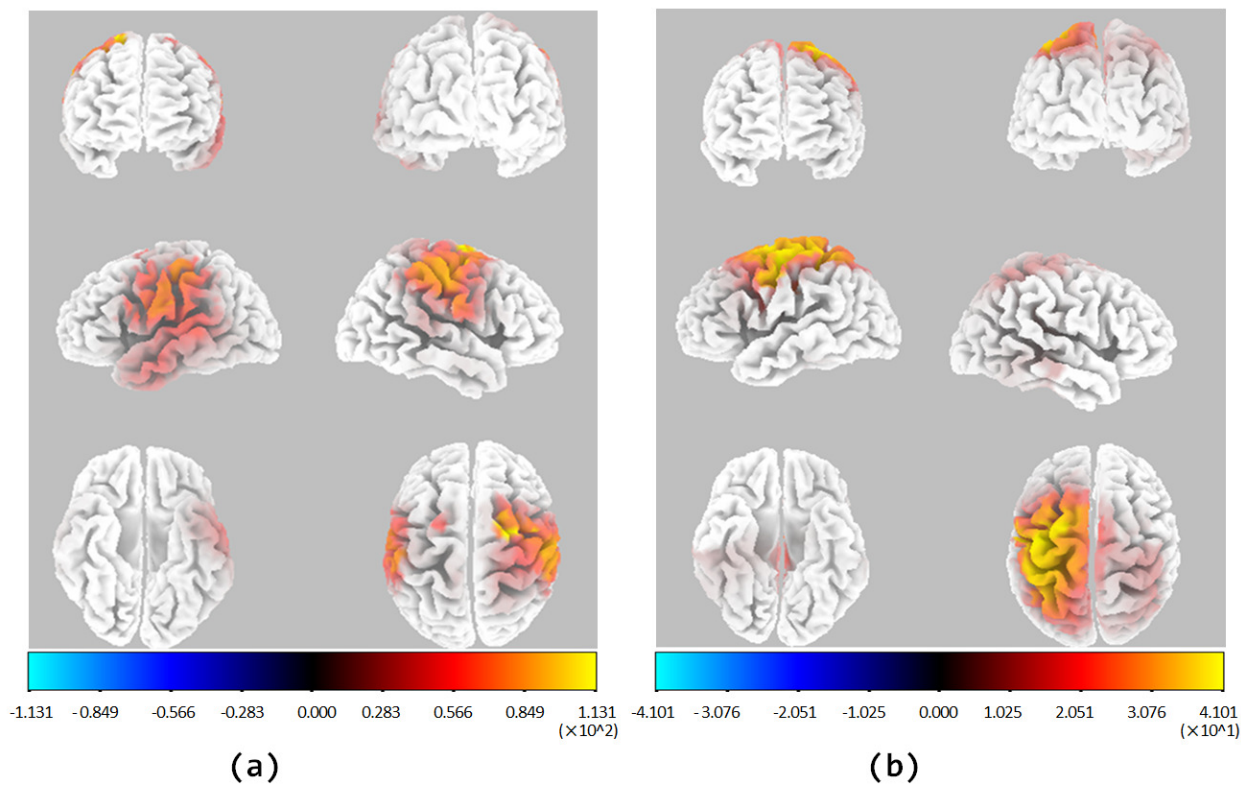
FIGURE 5. Regional brain activation obtained by EEG source analysis. (a) Left-hand imagery; (b) Right-hand imagery.
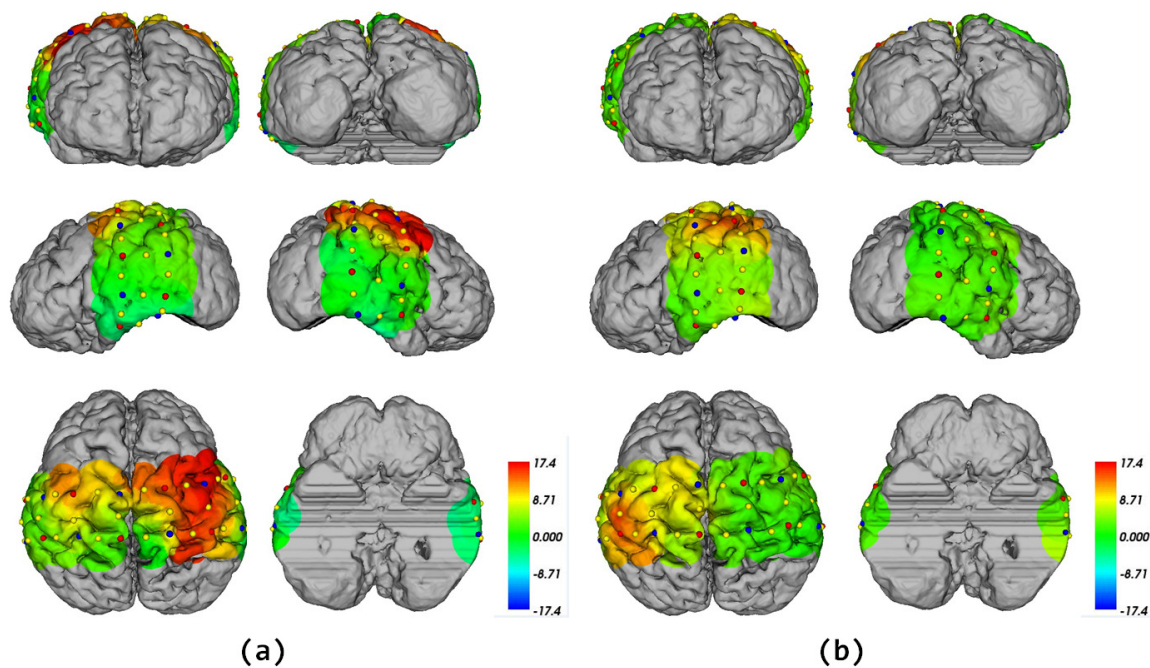
FIGURE 6. Regional brain activation obtained by fNIRS source analysis. (a) Left-hand imagery; (b) Right-hand imagery.

delay time. In the present study, the grid search method was used to optimize m and τ according to the classification accuracy. The search ranges for m and τ were set as [4:1:20] and [1:2:20], respectively. The optimal values of m and τ were determined over a space of [9 13] and [7 11], respectively. Next, the phase space for C3, Cz, and C4 was reconstructed

FIGURE 7. Signal processing procedure for the bimodal BCI.

with m and τ for each trial. The reconstructed phase space is shown by following trajectory matrix:

$$X_{PSR} = \begin{bmatrix} C_3 \\ C_z \\ C_4 \end{bmatrix} = \begin{bmatrix} C_{3\_1} & C_{3\_2} \dots C_{3\_M} \\ C_{z\_1} & C_{z\_2} \dots C_{z\_M} \\ C_{4\_1} & C_{4\_2} \dots C_{4\_M} \end{bmatrix} \quad (2)$$

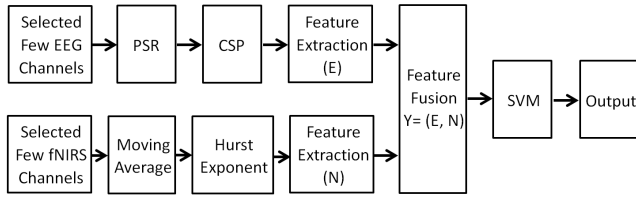By performing PSR, the original three-channel time-varying EEG data could be converted into $3*M$-channel time-varying signals. CSP is commonly used for effective multichannel feature extraction [54]–[56]. In the present study, CSP was used to extract features from the channel expanded EEG data X_{PSR} ($3*M$ channels) after channel expansion with PSR. The extracted features for motor imagery were defined as $Z = [Z_L, Z_R]$, where Z_L was the feature for the left-hand imagery and Z_R was the feature for the right-hand imagery. The extraction of Z_L and Z_R was performed as previously reported in [57].

The EEG feature vector for the two different conditions was defined as:

$$E_d = log(\frac{VAR_d}{\sum_{d=1}^{2} VAR_d}), \quad d = L, R \quad (3)$$

where VAR_d is the variance of Z among time points. A composite feature vector for the i-th trial EEG was defined as:

$$E_i = [E_{L\_i}, E_{R\_i}], \quad E_i \in R^{1 \times 2} \quad (4)$$

F. FNIRS FEATURE EXTRACTION

A moving average was applied to 4–10 s of HbO data (window length = 3/7 s) to remove the instant noise. For each trial, the Hurst exponent [58] for each channel was calculated and composes the fNIRS data feature N_i, which is defined as $N_i = [N_{c1\_i}, N_{c2\_i}, \dots, N_{c10\_i}], N_i \in R^{1 \times 10}$, where N_{cq_i} is the Hurst exponent for each channel, $q = 1, 2, \dots, 10$, indicates the q-th channel, $i = 1, 2, \dots, 60$, indicates the i-th trial.

G. DATA FUSION AND PATTERN CLASSIFICATION

The i-th EEG-fNIRS fusion feature was the combination of EEG feature and fNIRS feature, which was defined as:

$$\begin{aligned} Y_i &= [E_i, N_i] \\ &= [E_{L\_i}, E_{R\_i}, N_{c1\_i}, \dots, N_{c10\_i}], \quad Y_i \in R^{1 \times 12} \quad (5) \end{aligned}$$

The support vector machine (SVM) is a powerful and widely employed BCI classification method [17], [59]. It has high classification performance, relatively good scalability to

high-dimensional data, and explicit control of errors. In the present study, we used the C-support vector classification in the LIBSVM package [60] to implement SVM classification.

The basic concept of SVM is to determine the optimal decision hyperplane that best separates the data points into different classes with a maximum margin, whereas allowing errors during separation; i.e., map the input Y_i onto a high-dimensional feature space $z = \Phi(Y_i)$, and construct an optimal hyperplane defined by $w \cdot z + b = 0$ to separate examples into different classes, where w is the normal vector and b is the bias of the separation hyperplane. This is achieved by solving the primal problem:

$$min (\frac{1}{2} \|w\|^2 + C \sum_{i=1}^{n} \xi_i)$$
$$s.t. \ l_i(w \cdot z_i + b) \geq 1 - \xi_i, \xi_i \geq 0 \quad (6)$$

where l_i is the class label value of the i-th trial, n is the number of trials, ξ_i is the slack variable that allows an example to be in the margin or to be misclassified, and C is a penalty factor. This equation can be solved using Lagrange optimization; i.e., solving the quadratic programming (QP) problem, as follows:

$$max \ \sum_{i=1}^{n} a_i - \frac{1}{2} \sum_{i=1}^{n} \sum_{j=1}^{n} l_i l_j a_i a_j K(Y_i, Y_j)$$
$$s.t. \ \sum_{i=1}^{n} l_i a_i = 0, 0 \leq a_i \leq C \quad (7)$$

where a_i is the Lagrange multiplier from the QP problem, and $K(Y_i, Y_j)$ is the kernel function. Due to the nonlinear and small sample properties of EEG and fNIRS signals, we selected the radial basis kernel function (RBF) as the SVM kernel function:

$$K(Y_i, Y_j) = exp(-\gamma \|Y_i - Y_j\|^2), \gamma > 0 \quad (8)$$

where γ is the kernel parameter. The kernel parameter γ and penalty factor C are the main parameters that affect the performance of the SVM. γ determines the distribution of the transformed data in space, and the penalty factor C controls the trade-off between maximizing the margin and minimizing the training error, thus balancing classification violation and the margin. Therefore, γ and C are important for improving the correct rate and classification efficiency of the SVM. In the present study, we used the grid search method to optimize γ and C. The value ranges of γ and C were used as the grid edges, and different values of γ and C crossed over different grids. The optimal values for γ and C were found by searching on all of these grids. A two-step grid search was employed to reduce the computational complexity and accelerate the search speed, in which γ and C varied with a step of 2^p. In the first step, a coarse grid search was applied to determine the best region of demanded parameters. The initial search range for γ and C were set from 2^{-10} to 2^{10}, in which p was set as 2. In this step, we got a preliminary optimal value (γ_c and C_c). In the second step, a finer grid search was

TABLE 1. Comparison of participant classification accuracies for EEG, fNIRS, and bimodal EEG-fNIRS techniques.

Mode	Participants													
	ZJY	SXY	YQ	WK	ZZ	SLR	DWJ	WZY	TS	SGP	SYH	CZZ	Average	S.D.
EEG	100	86.7	76.7	70.0	66.7	66.7	63.3	58.3	70.0	83.3	75.0	80.0	74.7	11.5
fNIRS	55.0	54.7	79.2	52.5	59.0	60.2	55.8	43.1	52.7	57.3	55.6	56.7	56.8	8.3
EEG-fNIRS	100*	90.0*	78.3	81.7*	76.7*	75.0*	78.3*	75.0*	75.0*	86.7*	78.3*	80.0*	81.2	7.5

The accuracies were derived from data from three EEG channels (C3, Cz, C4) and 10 fNIRS channels.
*, bimodal accuracy higher than or equal to either single modality.

employed to recognize the final optimal γ and C. The search ranges were set as $[\gamma_c - 2^4, \gamma_c + 2^4]$ and $[C_c - 2^4, C_c + 2^4]$, respectively, in which p was set as 0.5. The optimal values of γ and C were obtained when the cross-validation accuracy was a maximum. In the present study, the optimum values of γ and C were determined over a space of $[2^{-7}\ 2^{-4}]$ and $[2^4\ 2^7]$, respectively.

To prevent the overfitting problem, a five-fold cross-validation approach was used in the present study. In one fold, each dataset was divided into five subsets with equal size. One of the subsets was used as a test set and the remaining four subsets were put together to form a training set. The optimal combination of γ and C was searched for to obtain maximum accuracy for the fold. This procedure was repeated five times (folds) and the average of the accuracies for all five folds was calculated to form the classification accuracy of this dataset.

By solving the QP problem, we calculated the fusion weight for each feature $w^* = \sum_{i=1}^{n} l_i a_i Y_i$, $b^* = l_i - \sum_{i=1}^{n} l_i a_i^*(Y_i \cdot Y_j)$, where $l_i a_i$ was the weight coefficient vector for each sample, and the number in $l_i a_i$ corresponded to the weight coefficient of the feature vector Y_i. For SVM, the data fusion and pattern classification were performed at the same time. The decision function can be described as:

$$f(Y) = sgn\{\sum_{i=1}^{n} l_i a_i^* K(Y, Y_i) + b^*\} \quad (9)$$

III. RESULTS

The classification accuracies for EEG, fNIRS, and EEG-fNIRS combinations for imagery tasks are shown in Table 1. Compared with the averaged accuracy of the single mode EEG, there was an average 6.5% increase in classification accuracy for the bimodal EEG-fNIRS. Compared with the average accuracy of the single mode fNIRS, there was an average 24.4% increase in classification accuracy for the bimodal EEG-fNIRS. To compare the classification effect among single mode EEG, single mode fNIRS, and bimodal EEG-fNIRS, we used one-way repeated measures ANOVA to test the difference between the averaged classification accuracies based on the three kinds of signals. We found that the main effect in the ANOVA was significant ($F = 32.0, p < 0.001$), meaning that there was a statistically significant difference between the three signals. Thus, post hoc tests were used to provide detailed information on which classification accuracies were significantly different from the others. Our results indicated that the averaged accuracy of the

bimodal EEG-fNIRS was significantly higher than that for both the single mode EEG and fNIRS (EEG-fNIRS vs. EEG, $p < 0.01$; EEG-fNIRS vs. fNIRS, $p < 0.001$). Moreover, the average classification accuracy for the single mode EEG was significantly higher than that for the single mode fNIRS ($p < 0.001$).

The averaged confusion matrices of all participants based on EEG, fNIRS and EEG-fNIRS are shown in Table 2, respectively. Compared with the single mode EEG and fNIRS, bimodal EEG-fNIRS has better classification performance.

TABLE 2. The averaged confusion matrices of all participants based on EEG, fNIRS and EEG-fNIRS.

Predicted Class		True Class		Sum
		Left Cue (30)	Right Cue (30)	
Predicted as Left		EEG: 23.5	EEG: 8.7	32.2
		fNIRS: 18.7	fNIRS: 14.6	33.3
		EEG-fNIRS: 25.1	EEG-fNIRS: 6.4	31.5
Predicted as Right		EEG: 6.5	EEG: 21.3	27.8
		fNIRS: 11.3	fNIRS: 15.4	26.7
		EEG-fNIRS: 4.9	EEG-fNIRS: 23.6	28.5

For each participant, the bimodal EEG-fNIRS was higher than (or equal to) that for the single mode EEG or fNIRS for all 12 participants, except for participant YQ; this case had an fNIRS accuracy higher than that for EEG accuracy.

The column charts of the accuracies of the single mode EEG and fNIRS plotted against the bimodal EEG-fNIRS for all participants are shown in Fig.8. These data show different classification accuracies for each participant. Participant ZJY showed the highest accuracy of 100% for the single mode EEG and the bimodal EEG-fNIRS, whereas participant WZY showed the lowest accuracy of 58.3% and 43.1% for the single mode EEG and fNIRS, respectively. The single mode fNIRS showed the lowest classification accuracy, whereas the bimodal EEG-fNIRS was optimal for almost all participants, except participant YQ. Our data suggest that there are large individual differences in classification accuracy of motor imagery. Thus, a BCI system with one mode may be inappropriate for participant with extremely low accuracy, whereas use of the bimodal system (e.g., participants ZZ, SLR, and WZY) can provide a higher classification accuracy.
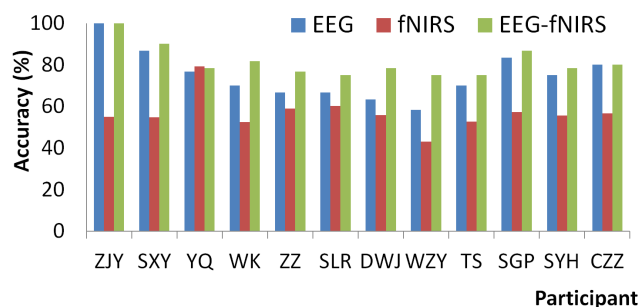
FIGURE 8. Classification accuracies for EEG, fNIRS, and EEG-fNIRS for all 12 participants.

IV. DISCUSSION

In the present study, we examined the performance of an EEG-fNIRS-based BCI for discrimination between a set of motor imagery tasks. EEG provides data on electrical cortical activity, whereas fNIRS monitors the oxygen metabolism of the cortex. Thus, this hybrid BCI system provides a more robust BCI signal that can improve the detection rate when compared to more conventional approaches. The majority of reported EEG-fNIRS hybrid BCI systems have used motor imagery tasks [37]–[39], [61], [62], although there are others based on P300 [63], spatial attention [64], selective sensation [65], memory load [66], [67], steady-state visual evoked potentials [35] and mental arithmetic [68]. The motor imagery task is a self-paced BCI paradigm that is controlled using a computer display. Compared with other mental tasks, motor imagery is relatively simple and stable. Moreover, motor imagery causes lateralization in fNIRS signals, which is useful for BCI classification [14], [19]. Thus, the motor imagery task is the traditional paradigm used for EEG-fNIRS hybrid BCI systems. In the present study, the motor imagery task provided high accuracy data, confirming its utility for EEG-fNIRS hybrid BCI devices.

EEG and fNIRS measure different physiological correlates of neural activity, and are susceptible to different noise sources. Recent studies using hybrid EEG-fNIRS BCIs suggest that simultaneous measurement of electrical and hemodynamic activity in the cerebral cortex provides more accurate BCI operation by combining features from both modalities [38]–[40], [61], [62], [64]. For example, Fazli *et al.* [39] reported that complementing EEG data with fNIRS improved motor imagery classification by approximately 5%. Lee *et al.* Reference [38] also demonstrated that EEG-fNIRS bimodal data increased the accuracy of classification by more than 10% for the motor imagery task. Further, Morioka *et al.* [64] reported that an EEG-fNIRS hybrid BCI improved spatial attention decoding accuracy by more than 8%. In the present study, there was an average 6.5% and 24.4% increase in classification accuracy for the bimodal EEG-fNIRS compared with single mode EEG and single mode fNIRS, respectively.

Similar to the previous EEG-fNIRS studies using motor imagery [37]–[39], [62], [69], the classification accuracy for single mode EEG was 74.7% in the present study, which is better than 56.8% for single mode fNIRS. Thus, in terms of classification accuracy, an fNIRS-based BCI on its own may not be a viable alternative to an EEG-based BCI. However, in combination with EEG, we found that fNIRS can significantly enhance BCI performance for most participants, as well as provide more accurate classification accuracy for participants otherwise unable to operate a solely EEG-based BCI. For example, participant WZY exhibited a classification accuracy of 58.3% and 43.1% for single mode EEG and fNIRS, respectively, which increased to 75.0% for bimodal EEG-fNIRS. Thus, for participants (and patients) unable to operate a single mode BCI, a bimodal EEG-fNIRS system may provide a viable alternative.

We suggest two main reasons for why the bimodal EEG-fNIRS-based BCI achieved better performance than that for single mode EEG and fNIRS. First, because every brain imaging method suffers from its particular limitations (e.g. EEG from spatial resolution; fNIRS from temporal resolution), EEG-fNIRS bimodal measurement is partly able to overcome these limitations by focusing on their individual strengths [39], [70]. Second, the combination of modalities can exhibit synergistic effects by exploiting the complementary information from multiple data sources. EEG collects the electrophysiological signals, whereas fNIRS collects the cerebral blood flow and oxygen metabolism signals from neural activity, respectively. These approaches complement each other both in quality (increases in the information sources) and quantity (increases in the data dimensionality). In the present study, we implement feature-level fusion by combining EEG and fNIRS features together, which provides more features for classification and reduces failure since interference does affect EEG and fNIRS signals simultaneously [71]. In the present study, we focused on motor imagery-based BCI. A number of previous studies have also confirmed that EEG-fNIRS combinations provide improved classification results for other event-related potential-based [72] and steady-state visual evoked potential (SSVEP)-based BCIs [35]. Thus, we consider bimodal EEG-fNIRS to be an effective method to improve classification performance in BCI applications.

In previous EEG-fNIRS BCI studies using motor imagery, most of them used large number of EEG-fNIRS channels. For example, Kaiser *et al.* [36] used six EEG electrodes and 52 fNIRS channels (17 emitters, 16 detectors) to achieve an average accuracy of 76.7%, Khan *et al.* [37] used six EEG electrodes and 17 fNIRS channels (six emitters, six detectors) to achieve an average accuracy of 66.0%, whereas Lee *et al.* [38] and Fazli *et al.* [39] used 37 EEG electrodes and 24 fNIRS channels (eight emitters, 16 detectors) covering the frontal, motor, and parietal areas, with an accuracy of 61.3% and 83.2%, respectively. Yu *et al.* [69] used 32 EEG electrodes and 64 fNIRS channels (32 emitters, 32 detectors) near the motor area to achieve an accuracy of 59.7% for EEG and 52.8% for fNIRS classification, whereas Almajidy *et al.* [73] used eight EEG electrodes and 20 fNIRS channels (eight emitters, eight detectors) to provide 77.0%

averaged accuracy. Further, Yin *et al.* [61] used 21 EEG electrodes and 24 fNIRS channels (10 emitters, eight detectors) to achieve 89.0% averaged accuracy. By comparison, In the present study, we used three EEG electrodes and 10 fNIRS channels (six emitters, six detectors), which provided 81.2% averaged accuracy.

Compared with previous reports, our study used the fewest EEG electrodes and fNIRS probes, but obtained the highest accuracy. This is likely due to the efficacy of our proposed PSR+CSP method, which uses PSR to reconstruct few-channel EEG signals into multichannel signals before sending them to CSP. Using the grid search method to optimize m and τ for PSR, the optimized reconstructed multichannel signals were obtained, which were combined with CSP to provide optimal results. Further, although the classification accuracy for the single mode fNIRS was not as high as that for EEG, the bimodal feature fusion of EEG and fNIRS features provided higher classification accuracy.

V. CONCLUSION

In the present study, we developed a highly accurate, few-channel, electroencephalograph (EEG) and functional near-infrared spectroscopy (fNIRS) bimodal BCI system. To improve the performance, we applied phase space reconstruction (PSR) to reconstruct the few-channel system into an equivalent multichannel system. After this transformation, common spatial pattern (CSP) was applied to the few-channel system. The EEG and fNIRS features were fused and classified with the support vector machine (SVM) method. The classification accuracy for the bimodal EEG-fNIRS system was 81.2%, which was 6.5% and 24.4% higher than that for the single mode EEG and fNIRS systems, respectively. We suggest that PSR+CSP is an effective method to obtain high classification accuracy for a few-channel BCI system.

REFERENCES

[1] L. M. Alonso-Valerdi, R. A. Salido-Ruiz, and R. A. Ramirez-Mendoza, "Motor imagery based brain–computer interfaces: An emerging technology to rehabilitate motor deficits," *Neuropsychologia*, vol. 79, pp. 354–363, Dec. 2015.

[2] P. Brunner, L. Bianchi, C. Guger, F. Cincotti, and G. Schalk, "Current trends in hardware and software for brain-computer interfaces (BCIs)," *J. Neural Eng.*, vol. 8, no. 2, p. 025001, Apr. 2011.

[3] L. F. Nicolas-Alonso and J. Gomez-Gil, "Brain computer interfaces, a review," *Sensors (Basel)*, vol. 12, no. 12, pp. 1211–1279, Sep. 2012.

[4] A. Turnip and K. S. Hong, "Classifying mental activities from EEG-P300 signals using adaptive neural network," *Int. J. Innov. Comput. Innov. Comput., Inf. Control: IJICIC*, vol. 8, no. 9, pp. 6429–6443, Sep. 2012.

[5] S. Moghimi, A. Kushki, A. M. Guerguerian, and T. Chau, "A review of EEG-based brain-computer interfaces as access pathways for individuals with severe disabilities," *Assist Technol.*, vol. 25, no. 2, pp. 99–110, Apr. 2013.

[6] M. Hamedi, S. H. Salleh, and A. M. Noor, "Electroencephalographic motor imagery brain connectivity analysis for BCI: A review," *Neural Comput.*, vol. 28, no. 6, pp. 999–1041, Jun. 2016.

[7] Y. Zhang, G. Zhou, J. Jin, Q. Zhao, X. Wang, and A. Cichocki, "Sparse Bayesian classification of EEG for brain–computer interface," *IEEE Trans. Neural Netw. Learn. Syst.*, vol. 27, no. 11, pp. 2256–2267, Nov. 2016.

[8] S. T. Foldes, D. J. Weber, and J. L. Collinger, "MEG-based neurofeedback for hand rehabilitation," *J. Neuroeng. Rehabil.*, vol. 12, p. 85, Sep. 2015.

[9] J. Mellinger *et al.*, "An MEG-based brain-computer interface (BCI)," *Neuroimage*, vol. 36, no. 3, pp. 581–593, Jul. 2007.

[10] R. Sitaram, A. Caria, and N. Birbaumer, "Hemodynamic brain–computer interfaces for communication and rehabilitation," *Neural Netw.*, vol. 22, no. 9, pp. 1320–1328, Nov. 2009.

[11] S. Ruiz, K. Buyukturkoglu, M. Rana, N. Birbaumer, and R. Sitaram, "Real-time fMRI brain computer interfaces: Self-regulation of single brain regions to networks," *Biol. Psychol.*, vol. 95, pp. 4–20, Jan. 2014.

[12] N. Naseer and K. S. Hong, "fNIRS-based brain-computer interfaces: A review," *Frontiers Human Neurosci.*, vol. 9, p. 3, Jan. 2015.

[13] S. Weyand, K. Takehara-Nishiuchi, and T. Chau, "Weaning off mental tasks to achieve voluntary self-regulatory control of a near-infrared spectroscopy brain-computer interface," *IEEE Trans. Neural Syst. Rehabil. Eng.*, vol. 23, no. 4, pp. 548–561, Jul. 2015.

[14] R. Sitaram *et al.*, "Temporal classification of multichannel near-infrared spectroscopy signals of motor imagery for developing a brain-computer interface," *Neuroimage*, vol. 34, no. 4, pp. 1416–1427, Feb. 2007.

[15] Y. Hoshi, "Functional near-infrared spectroscopy: current status and future prospects," *J. Biomed. Opt.*, vol. 12, no. 6, p. 062106, Nov./Dec. 2007.

[16] M. Ferrari and V. Quaresima, "A brief review on the history of human functional near-infrared spectroscopy (fNIRS) development and fields of application," *Neuroimage*, vol. 63, no. 2, pp. 921–935, Nov. 2012.

[17] N. Naseer, N. K. Qureshi, F. M. Noori, and K.-S. Hong, "Analysis of different classification techniques for two-class functional near-infrared spectroscopy-based brain-computer interface," *Comput. Intell. Neurosci.*, vol. 2016, Sep. 2016, Art. no. 5480760.

[18] N. K. Logothetis, J. Pauls, M. Augath, T. Trinath, and A. Oeltermann, "Neurophysiological investigation of the basis of the fMRI signal," *Nature*, vol. 412, pp. 150–157, Jul. 2001.

[19] S. Coyle, T. Ward, C. Markham, and G. McDarby, "On the suitability of near-infrared (NIR) systems for next-generation brain-computer interfaces," *Physiol. Meas.*, vol. 25, no. 4, pp. 815–822, Aug. 2004.

[20] S. M. Coyle, T. E. Ward, and C. M. Markham, "Brain-computer interface using a simplified functional near-infrared spectroscopy system," *J. Neural Eng.*, vol. 4, no. 3, pp. 219–226, Sep. 2007.

[21] N. Naseer and K.-S. Hong, "Classification of functional near-infrared spectroscopy signals corresponding to the right- and left-wrist motor imagery for development of a brain–computer interface," *Neurosci. Lett.*, vol. 553, pp. 84–89, Oct. 2013.

[22] P. Horki, T. Solis-Escalante, C. Neuper, and G. Müller-Putz, "Combined motor imagery and SSVEP based BCI control of a 2 DoF artificial upper limb," *Med. Biol. Eng. Comput.*, vol. 49, no. 5, pp. 567–577, May 2011.

[23] R. Beisteiner, P. Hollinger, G. Lindinger, W. Lang, and A. Berthoz, "Mental representations of movements. Brain potentials associated with imagination of hand movements," *Electroencephalogr. Clin. Neurophysiol.*, vol. 96, no. 2, pp. 183–193, Mar. 1995.

[24] G. Pfurtscheller, C. Brunner, A. Schlögl, and F. H. Lopes da Silva, "Mu rhythm (de)synchronization and EEG single-trial classification of different motor imagery tasks," *Neuroimage*, vol. 31, no. 1, pp. 153–159, May 2006.

[25] G. Pfurtscheller and C. Neuper, "Motor imagery and direct brain-computer communication," *Proc. IEEE*, vol. 89, no. 7, pp. 1123–1134, Jul. 2001.

[26] A. Schlogl, F. Lee, H. Bischof, and G. Pfurtscheller, "Characterization of four-class motor imagery EEG data for the BCI-competition 2005," *J. Neural Eng.*, vol. 2, no. 4, pp. L14–L22, Dec. 2005.

[27] E. Thomas, M. Dyson, and M. Clerc, "An analysis of performance evaluation for motor-imagery based BCI," *J. Neural Eng.*, vol. 10, no. 3, p. 031001, Jun. 2013.

[28] Y. Zhang, Y. Wang, J. Jin, and X. Wang, "Sparse Bayesian learning for obtaining sparsity of EEG frequency bands based feature vectors in motor imagery classification," *Int. J. Neural Syst.*, vol. 11, p. 1650032, Apr. 2016.

[29] T. Nagaoka *et al.*, "Development of a new rehabilitation system based on a brain-computer interface using near-infrared spectroscopy," *Adv. Exp. Med. Biol.*, vol. 662, pp. 497–503, Jan. 2010

[30] S. D. Power, A. Kushki, and T. Chau, "Towards a system-paced near-infrared spectroscopy brain-computer interface: Differentiating prefrontal activity due to mental arithmetic and mental singing from the no-control state," *J. Neural Eng.*, vol. 8, no. 6, p. 066004, Dec. 2011.

[31] L. C. Schudlo and T. Chau, "Dynamic topographical pattern classification of multichannel prefrontal NIRS signals: II. Online differentiation of mental arithmetic and rest," *J. Neural Eng.*, vol. 11, no. 1, p. 016003, Feb. 2014.

[32] S. Takahashi, H. Nakamura, and H. Tsunashima, "Multichannel temporal data classification of motor imagination using fNIRS," in *Proc. ICCAS*, Gyeonggi-Do, South Korea, 2010, pp. 2443–2447.

[33] B. Koo *et al.*, "A hybrid NIRS-EEG system for self-paced brain computer interface with online motor imagery," *J. Neurosci. Methods*, vol. 244, pp. 26–32, Apr. 2015.

[34] M. J. Khan, M. J. Hong, and K. S. Hong, "Decoding of four movement directions using hybrid NIRS-EEG brain-computer interface," *Frontiers Human Neurosci.*, vol. 8, p. 244, Apr. 2014.

[35] Y. Tomita, F. B. Vialatte, G. Dreyfus, Y. Mitsukura, H. Bakardjian, and A. Cichocki, "Bimodal BCI using simultaneously NIRS and EEG," *IEEE Trans. Biomed. Eng.*, vol. 61, no. 4, pp. 1274–1284, Apr. 2014.

[36] V. Kaiser *et al.*, "Cortical effects of user training in a motor imagery based brain-computer interface measured by fNIRS and EEG," *Neuroimage*, vol. 85, pp. 432–444, Jan. 2014.

[37] M. J. Khan, K.-S. Hong, N. Naseer, and M. R. Bhutta, "Motor imagery performance evaluation using hybrid EEG-NIRS for BCI," in *Proc. SICE*, Hangzhou, China, 2015, pp. 1150–1155.

[38] M. H. Lee, S. Fazli, J. Mehnert, and S. W. Lee, "Subject-dependent classification for robust idle state detection using multi-modal neuroimaging and data-fusion techniques in BCI," *Pattern Recognit.*, vol. 48, no. 8, pp. 2725–2737, Aug. 2015.

[39] S. Fazli *et al.*, "Enhanced performance by a hybrid NIRS-EEG brain computer interface," *Neuroimage*, vol. 59, no. 1, pp. 519–529, Jan. 2012.

[40] A. P. Buccino, H. O. Keles, and A. Omurtag, "Hybrid EEG-fNIRS asynchronous brain-computer interface for multiple motor tasks," *PLoS ONE*, vol. 11, no. 1, p. e0146610, 2016.

[41] M. Kilintari, S. Narayana, A. Babajani-Feremi, R. Rezaie, and A. C. Papanicolaou, "Brain activation profiles during kinesthetic and visual imagery: An fMRI study," *Brain Res.*, vol. 1646, pp. 249–261, Sep. 2016.

[42] S. C. Wriessnegger, D. Steyr, K. Koschutnig, and G. R. Muller-Putz, "Cooperation in mind: Motor imagery of joint and single actions is represented in different brain areas," *Brain Cognit.*, vol. 109, pp. 19–25, Nov. 2016.

[43] L. Gagnon *et al.*, "Quantification of the cortical contribution to the NIRS signal over the motor cortex using concurrent NIRS-fMRI measurements," *Neuroimage*, vol. 59, no. 4, pp. 3933–3940, Feb. 2012.

[44] A. Cichocki and S. I. Amari, *Adaptive Blind Signal and Image Processing: Learning Algorithms and Applications*. Hoboken, NJ, USA: Wiley, 2003. [Online]. Available: http://www.bsp.brain.riken.jp/ICALAB

[45] W. Zhou and J. Gotman, "Automatic removal of eye movement artifacts from the EEG using ICA and the dipole model," *Progr. Natural Sci.*, vol. 19, no. 9, pp. 1165–1170, Sep. 2009.

[46] A. Flexer, H. Bauer, J. Pripfl, and G. Dorffner, "Using ICA for removal of ocular artifacts in EEG recorded from blind subjects," *Neural Netw.*, vol. 18, no. 7, pp. 998–1005, Sep. 2005.

[47] R. D. Pascual-Marqui, "Standardized low-resolution brain electromagnetic tomography (sLORETA): technical details," *Methods Find Exp. Clin. Pharmacol.*, vol. 24, pp. 5–12, 2002. [Online]. Available: http://www.uzh.ch/keyinst/loreta.htm

[48] V. L. Towle *et al.*, "The spatial location of EEG electrodes: Locating the best-fitting sphere relative to cortical anatomy," *Electroencephalogr. Clin. Neurophysiol.*, vol. 86, no. 1, pp. 1–6, Jan. 1993.

[49] T. N. Lal *et al.*, "Support vector channel selection in BCI," *IEEE Trans. Biomed. Eng.*, vol. 51, no. 6, pp. 1003–1010, Jun. 2004.

[50] M. B. Kennel, R. Brown, and H. D. I. Abarbanel, "Determining embedding dimension for phase-space reconstruction using a geometrical construction," *Phys. Rev. A*, vol. 45, no. 6, pp. 3403–3411, Mar. 1992.

[51] C. Guger, H. Ramoser, and G. Pfurtscheller, "Real-time EEG analysis with subject-specific spatial patterns for a brain-computer interface (BCI)," *IEEE Trans. Rehabil. Eng.*, vol. 8, no. 4, pp. 447–456, Dec. 2000.

[52] R. Djemal, A. G. Bazyed, K. Belwafi, S. Gannouni, and W. Kaaniche, "Three-class EEG-based motor imagery classification using phase-space reconstruction technique," *Brain Sci.*, vol. 6, no. 3, p. E36, Aug. 2016.

[53] M. Chen, Y. Fang, and X. Zheng, "Phase space reconstruction for improving the classification of single trial EEG," *Biomed. Signal Process.*, vol. 11, no. 5, pp. 10–16, May 2014.

[54] Y. Zhang, G. Zhou, J. Jin, X. Wang, and A. Cichocki, "Optimizing spatial patterns with sparse filter bands for motor-imagery based brain–computer interface," *J. Neurosci. Methods*, vol. 255, pp. 85–91, Nov. 2015.

[55] K. K. Ang, Z. Y. Chin, C. Wang, C. Guan, and H. Zhang, "Filter bank common spatial pattern algorithm on BCI competition IV datasets 2a and 2b," *Frontiers Neurosci.*, vol. 6, no. 1, p. 39, Mar. 2012.

[56] B. Blankertz, R. Tomioka, S. Lemm, M. Kawanabe, and K. R. Müller, "Optimizing spatial filters for robust EEG single-trial analysis," *IEEE Signal Process. Mag.*, vol. 25, no. 1, pp. 41–56, Jan. 2008.

[57] S. Ge, R. Wang, and D. Yu, "Classification of four-class motor imagery employing single-channel electroencephalography," *PLoS ONE*, vol. 9, no. 6, p. e98019, Jun. 2014.

[58] S. Vorobyov and A. Cichocki, "Blind noise reduction for multisensory signals using ICA and subspace filtering, with application to EEG analysis," *Biol. Cybern.*, vol. 86, no. 4, pp. 293–303, May 2002.

[59] C. Cortes and V. Vapnik, "Support-vector networks," *Mach. Learn.*, vol. 20, no. 3, pp. 273–297, Sep. 1995.

[60] C. C. Chang and C. J. Lin, "LIBSVM: A library for support vector machines," *ACM Trans. Intell. Syst. Technol.*, vol. 2, no. 3, Apr. 2011, Art. no. 27.

[61] X. Yin *et al.*, "A hybrid BCI based on EEG and fNIRS signals improves the performance of decoding motor imagery of both force and speed of hand clenching," *J. Neural Eng.*, vol. 12, no. 3, p. 036004, Jun. 2015.

[62] Y. Blokland *et al.*, "Combined EEG-fNIRS decoding of motor attempt and imagery for brain switch control: An offline study in patients with tetraplegia," *IEEE Trans. Neural Syst. Rehabil. Eng.*, vol. 22, no. 2, pp. 222–229, Mar. 2014.

[63] C. N. Gupta and R. Palaniappan, "Using EEG and NIRS for brain-computer interface and cognitive performance measures: A pilot study," *Int. J. Chem. Phys. Sci.*, vol. 1, no. 1, pp. 69–81, Jan. 2013.

[64] H. Morioka *et al.*, "Decoding spatial attention by using cortical currents estimated from electroencephalography with near-infrared spectroscopy prior information," *Neuroimage*, vol. 90, pp. 128–139, Apr. 2014.

[65] X. Shu, L. Yao, X. Sheng, and D. Zhang, "A hybrid BCI study: Temporal optimization for EEG single-trial classification by exploring hemodynamics from the simultaneously measured NIRS data," in *Proc. IEEE ROBIO*, Bali, Indonesia, 2014, pp. 914–918.

[66] V. Lai *et al.*, "A normal intensity level of psycho-physiological stress can benefit working memory performance at high load," *Int. J. Ind. Ergonomics*, vol. 44, no. 3, pp. 362–367, May 2014.

[67] L. M. Hirshfield *et al.*, "Combining electroencephalograph and functional near infrared spectroscopy to explore users' mental workload," in *Foundations of Augmented Cognition. Neuroergonomics and Operational Neuroscience* (Lecture Notes in Computer Science), vol. 5638. 2009, pp. 239–247.

[68] K. Oyama and K. Sakatani, "Temporal comparison between NIRS and EEG signals during a mental arithmetic task evaluated with self-organizing maps," *Adv. Exp. Med. Biol.*, vol. 923, pp. 223–229, Aug. 2016

[69] J. Yu, K. A. Kai, C. Guan, and C. Wang, "A multimodal fNIRS and EEG-based BCI study on motor imagery and passive movement," in *Proc. 6th IEEE/EMBS NER*, San Diego, CA, USA, Nov. 2013, pp. 5–8.

[70] F. Biessmann, S. Plis, F. C. Meinecke, T. Eichele, and K. R. Müller, "Analysis of multimodal neuroimaging data," *IEEE Rev. Biomed. Eng.*, vol. 4, pp. 26–58, Jan. 2011.

[71] K. Geetha and V. Radhakrishnan, "Multimodal biometric system: A feature level fusion approach," *Int. J. Comput. Appl.*, vol. 71, no. 4, pp. 25–29, Jun. 2013.

[72] E. B. J. Coffey, A. M. Brouwer, and J. B. F. van Erp, "Measuring workload using a combination of electroencephalography and near infrared spectroscopy," *Proc. Human Factors Ergonomics Soc. Annu. Meeting*, vol. 56, no. 1, pp. 1822–1826, Sep. 2012.

[73] R. K. Almajidy, Y. Boudria, U. G. Hofmann, W. Besio, and K. Mankodiya, "Multimodal 2D brain computer interface," in *Proc. 37th Annu. Int. Conf. IEEE Eng. Med. Biol. Soc. (EMBC)*, Aug. 2015, pp. 1067–1070.

SHENG GE received the B.E. degree from the Nanjing University of Science and Technology, China, in 1997, and the M.E. and Ph.D. degrees from Yamaguchi University, Japan, in 2001 and 2004, respectively. From 2004 to 2005, he was a Research Assistant with the Faculty of Engineering, Yamaguchi University. From 2005 to 2007, he was a COE Research Fellow with the Graduate School of Information Science and Electrical Engineering, Kyushu University, where he was an Assistant Professor in 2007. From 2007 to 2009, he was a Post-Doctoral Fellow with the Department of Radiology, University of California at San Diego, La Jolla, USA. From 2010 to 2012, he was an Associate Professor with the Nanjing University of Science and Technology, China. Since 2010, he has been an Associate Professor with the Key Laboratory of Child Development and Learning Science, Ministry of Education, Research Center for Learning Science, Southeast University, China. His current research interests include brain science, cognitive science, and biomedical signal processing.
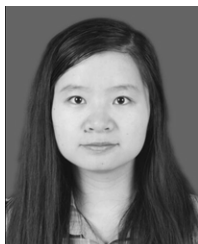
QING YANG received the B.E. degree in automation and the M.E. degree in neural information engineering from Southeast University, China, in 2013 and 2016, respectively. Since 2016, she has been an Algorithm Development Engineer with Dianping.com.

RUIMIN WANG received the B.E. degree in communication engineering from the Chengdu University of Information Technology, China, in 2009, and the M.E. degree in signal and information processing from the Nanjing University of Science and Technology, China, in 2015. From 2015 to 2016, she visited the Graduate School of Systems Life Sciences, Kyushu University, Japan, as a Research Student, and now she is pursuing the Ph.D. degree with Kyushu University, Japan. Her current interests include brain information processing and functional brain mapping.

PAN LIN received the Ph.D. degree in biomedical engineering from Xi'an Jiaotong University, China, in 2015. From 2007 to 2011, he was a Post-Doctoral Researcher with the center for Mind/Brain sciences, University of Trento, Italy. From 2013 to 2014, he was a Research Fellow with the Harvard Medical School, McLean Hospital, USA. Since 2011, he has been an Associate Professor with the Institute of Biomedical Engineering, Xi'an Jiaotong University. His current research interests include multimodal neuroimaging, brain signal processing, and machine learning.

JUNFENG GAO received the Ph.D. degree in biomedical engineering from Xi'an Jiaotong University, China, in 2011. He is currently an Associate Professor with the College of Biomedical Engineering, South-Central of University for Nationalities, China. His current research interests include feature selection methods, machine learning algorithms, pattern recognition, brain signal processing, and the investigation of neurophysiological mechanisms of human brain activity using EEG and functional MRI.

YUE LENG received the B.E. and Ph.D. degrees from Southeast University, China, in 2003 and 2011, respectively. From 2008 to 2009, she was a Visiting Student with the Department of Psychology, University of Southern California, USA. Since 2011, she has been an Assistant Professor with the Key Laboratory of Child Development and Learning Science, Ministry of Education, Research Center for Learning Science, Southeast University, China. Her current research interests include cognitive neuroscience and social cognition.
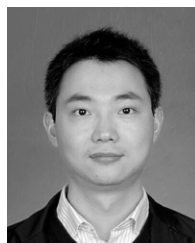
YUANKUI YANG received the B.E., M.E., and Ph.D. degrees from Southeast University, China, in 2004, 2007, and 2011, respectively. Since 2011, he has been a Lecturer with the Key Laboratory of Child Development and Learning Science, Ministry of Education, Research Center for Learning Science, Southeast University, China. His current research interests include brain science, cognitive science, and biomedical signal processing.

HAIXIAN WANG (M'09–SM'16) received the B.S. and M.S. degrees in statistics and the Ph.D. degree in computer science from Anhui University, Hefei, China, in 1999, 2002, and 2005, respectively. From 2002 to 2005, he was with the Key Laboratory of Intelligent Computing and Signal Processing, Ministry of Education of China. He is currently with the Key Laboratory of Child Development and Learning Science, Ministry of Education, Research Center for Learning Science, Southeast University, China. His research interests include EEG signal processing, statistical pattern recognition, and machine learning.

• • •